

Shortcuts to Adiabaticity for Fast Qubit Readout in Circuit Quantum Electrodynamics

F. A. Cárdenas-López¹ and Xi Chen^{2,3,*}

¹International Center of Quantum Artificial Intelligence for Science and Technology (QuArtist) and Physics Department, Shanghai University, 200444 Shanghai, China

²Department of Physical Chemistry, University of the Basque Country UPV/EHU, Bilbao, Spain

³EHU Quantum Center, University of the Basque Country UPV/EHU, 48940 Leioa, Spain

We propose how to engineer the longitudinal coupling to accelerate the measurement of a qubit longitudinally coupled to a cavity, motivated by the concept of shortcuts to adiabaticity. Different modulations are inversely designed from inverse engineering, counter-diabatic driving and genetic algorithm, for achieving optimally large values of the signal-to-noise ratio (SNR) at nanosecond scale. By comparison, we demonstrate that our protocols outperform the usual periodic modulations on the pointer state separation and SNR. Finally, we show a possible implementation considering state-of-the-art circuit quantum electrodynamics architecture, estimating the minimal time allowed for the measurement process.

I. INTRODUCTION

Retrieving information from a quantum system is at the heart of quantum information processing applications, in which an accurate and reliable quantum measurement is requisite. The most common measurement strategy is dispersive readout consisting in coupling an auxiliary system whose observables depend on the system state. Specifically, in superconducting quantum circuit (SC) or circuit quantum electrodynamics (cQED) [1–15], the qubit measurement is carried out through an auxiliary oscillator whose frequency relies on the qubit state [16–20]. However, dispersive readout has the drawback that its performance is limited by the detuning between the qubit and the oscillator which bounds the number of thermal photons and induces losses via Purcell effect as well [21–23]. A way to circumvent this limitation relies on engineer the longitudinal interaction between the quantum systems [24–27] yielding the non-demolition quantum measurement that is faster and more robust than the previous dispersive approach. Moreover, the parametric modulation of the external magnetic flux on a cavity-qubit system leads to rapid and unconditional reset mechanism [28].

In the past decade, shortcuts to adiabaticity (STA) [29] have experienced a huge development, with the various applications of quantum computing and more generally quantum technologies [30]. The methods of STA provide efficient control of quantum systems, by accelerating the slow adiabatic processes, and overcoming obstacles from systematic errors or environmental noise, see review [30]. Recently, STA have been generalized to complex open systems [31, 32], which offer the opportunity for designing a counter-diabatic pulse, to accelerate a dissipative process in cQED [33].

In this article, we propose STA method for elaborating the modulation of longitudinal coupling between a two-level system with a cavity mode to accelerate the qubit measurement. By using inverse engineering, we obtain large values for the cavity pointer state separation and the signal-to-noise ratio (SNR) on a short timescale. Besides, the SNR is exponentially enhanced when the cavity is prepared in a squeezed state. For

completeness, we further discuss the measurement process speed-up by counter-diabatic driving, and their possible implementations. Moreover, we use genetic algorithm, a search-based optimization technique, to find optimal or near-optimal modulation. Finally, a feasible experimental model regarding state-of-the-art cQED architecture is considered and the minimal time for the measurement process is estimated with the bound of coupling strength.

II. LONGITUDINAL CAVITY-QUBIT INTERACTION

We consider an LC oscillator of frequency ω_r longitudinally coupled to a two-level system of frequency ω_q with time-dependent coupling strength $g_z(t)$ described through the Hamiltonian [26] ($\hbar = 1$)

$$\mathcal{H} = \frac{\omega_q}{2} \sigma^z + \omega_r \hat{a}^\dagger \hat{a} + g_z(t) \sigma^z (\hat{a}^\dagger + \hat{a}). \quad (1)$$

Here σ^z is the z -component Pauli matrix describing the two-level system, and a^\dagger (a) is the creation (annihilation) operator of the LC oscillator. This Hamiltonian corresponds to a state-dependent displaced oscillator. When the cavity acts as a pointer state, we can perform high-fidelity quantum measurement on the qubit state since the cavity state displaces upwards or downwards on its phase state according to the qubit state. Furthermore, as the longitudinal interaction commutes with the free terms of the Hamiltonian such process is a quantum nondemolition measurement (QND) [26].

We aim to engineer $g_z(t)$ inversely to accelerate the QND measurement process. For doing so, we propose a solution for the Schrödinger equation of \mathcal{H} as $|\Psi(x, t)\rangle = e^{-iE_{LC}t/\hbar} \mathcal{V}(t) |\varphi(x, t)\rangle |\xi\rangle$, where $E_{LC} = \omega_r(n + 1/2)$ and $|\varphi(x, t)\rangle$ correspond to the eigenenergies and eigenfunctions of the LC oscillator $\mathcal{H}_{LC} = \omega_r \hat{a}^\dagger \hat{a}$. Besides, $|\xi\rangle$ describes the qubit state. As a consequence, $\mathcal{V}(t) = e^{i\theta(t)} e^{-i\dot{g}_c(t)\sigma^z(a^\dagger+a)/\omega_r^2} e^{-g_c(t)\sigma^z(a^\dagger-a)/\omega_r}$ is a unitary transformation that eliminates the longitudinal coupling [34], where $\theta(t) = -\int_0^t \mathcal{L}_g(t') dt'$ corresponds to a phase relating the coupling strength $g_z(t)$ with the auxiliary variable $g_c(t)$ through the Lagrangian

$$\mathcal{L}_g(t) = \frac{\dot{g}_c^2(t)}{\omega_r^3} - \frac{g_c^2(t)}{\omega_r} + \frac{2g_c(t)g_z(t)}{\omega_r}. \quad (2)$$

* chenxi1979cn@gmail.com

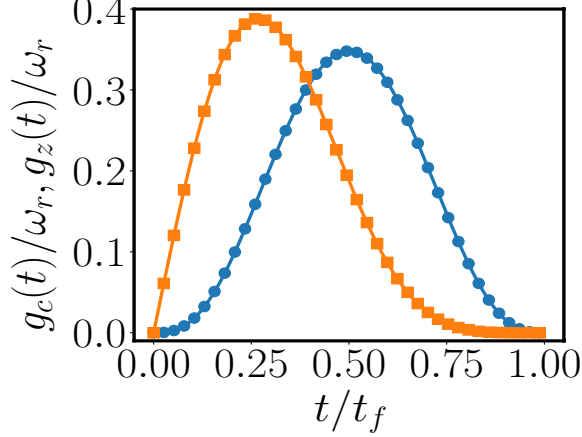


FIG. 1. Coupling strength modulation $g_c(t)$ and $g_z(t)$ calculated with the reserve engineering approach. Blue and orange solid line stand for $g_c(t)$ for the polynomial and trigonometric ansätze, respectively, whereas blue dots and orange squares corresponds to $g_z(t)$. We have performed the simulation with the parameters $\kappa/2\pi = 1$ MHz, $g_{z0}/2\pi = 21$ MHz, $\omega_r/2\pi = 6.6$ GHz for a designed time $t_f = \pi/(100\kappa)$ [26].

To guarantee that $|\Psi(x, t)\rangle$ corresponds to the exact solution of the time-dependent Schrödinger equation, the classical variables must obey the equation of motion, (see Appendix A for the detailed calculation)

$$\ddot{g}_c(t) + \omega_r^2 [g_c(t) - g_z(t)] = 0, \quad (3)$$

which is nothing but the Euler-Lagrange equation from Eq. (2). In what follow, we use Eq. (3) to engineer inversely the modulation of suitable coupling strength $g_z(t)$, in order to accelerate measurement process.

Sharing the concept of STA [29], we require that $g_c(t)$ fulfill the following boundary conditions [35]:

$$g_c(0) = 0; g_c(t_f) = 0, \quad (4a)$$

$$\dot{g}_c(0) = \ddot{g}_c(0) = \dot{g}_c(t_f) = \ddot{g}_c(t_f) = 0. \quad (4b)$$

The flexibility left in the inverse-engineering approach permits us to add a constrain over the final cavity displacement i.e.,

$$\int_0^{t_f} g_c(s) ds = g_{z0}\pi/(2\kappa). \quad (5)$$

There exist a vast number of function fulfilling the above criteria, we suggest a polynomial ansätze of the form $g_c(t) = \sum_{\ell=0}^6 b_\ell t^\ell$ that leads to

$$g_c(t) = -\frac{70\pi g_{z0} t^3 (t - t_f)^3}{\kappa t_f^7}. \quad (6)$$

However, this is not the unique solution for Eq. (3) with the initial and final boundary conditions, see Eqs. (4a), (4b) and (5). For the generality, we assume an alternative trigonometric

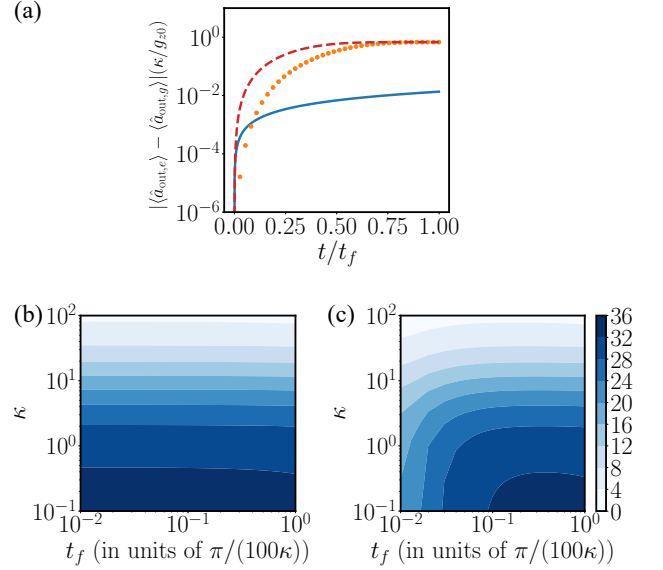


FIG. 2. (a) Relative pointer state separation for the output cavity field \hat{a}_{out} as function of t/t_f for the inverse engineering with polynomial (orange dotted) and trigonometric (red dashed) ansätze for longitudinal coupling strength. We compare with the case with the conventional sinusoidal modulation (blue solid). Function $F(\kappa, t_f)$ as a function of the decay rate and the final time t_f for both polynomial (b) and trigonometric (c) modulations. All parameters are the same as those in Fig. 2.

ansätze of the form $g_c(t) = \sum_m^6 \mathcal{A}_m(t) \sin(m\pi t/t_f)$, resulting in

$$g_c(t) = \frac{3g_{z0}\pi^2}{2\kappa t_f} \sin\left(\frac{\pi t}{2t_f}\right) \cos^5\left(\frac{\pi t}{2t_f}\right). \quad (7)$$

Consequently, we obtain $g_z(t)$ by substituting $g_c(t)$ into Eq. (3), as illustrated in Fig. 1, where the experimental parameters in an realistic cQED [26] yield $g_z(t) \simeq g_c(t)$ for large frequency ω_r of LC oscillator, and the measuring time t_f can be shortened if the larger coupling strength is allowed.

III. QUBIT READOUT

Now, we consider the evolution of the pointer state with the modulation of $g_c(t)$ given in Eqs. (6) and (7). The dynamical equation of the cavity field regarding losses [36] reads $\dot{\hat{a}} = ig_c(t)\sigma^z - \kappa\hat{a}/2 - \sqrt{\kappa}\hat{a}_{\text{in}}$, where κ is the decay rate of the LC oscillator, and \hat{a}_{in} is the input cavity operator taking into account the effect of an additional subsystem (measurement apparatus). By assuming both \hat{a}_{in} and \hat{a} are in their vacuum state, the solution of this equation yields

$$\langle \hat{a}(t) \rangle = -i\langle \sigma^z \rangle e^{-\kappa t/2} \int_0^t g_c(s) e^{\kappa s/2} ds. \quad (8)$$

Depending on the value of $\langle \sigma^z \rangle$, the field will be displaced upward or downward on the phase space. To quantify this

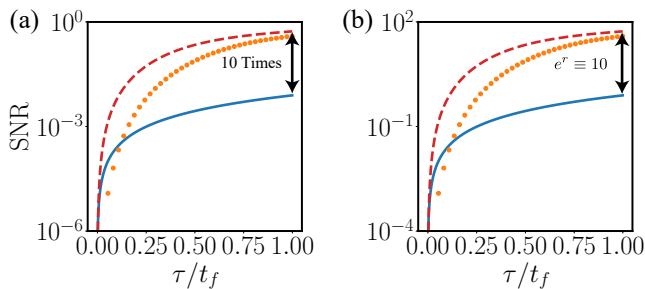


FIG. 3. Signal-to-noise ratio (SNR) as function of the dimensionless measuring time τ/t_f (a) regarding both sinusoidal modulation (blue solid) and the inverse-engineered protocol with polynomial (orange dotted) and trigonometric (red dashed) ansatzes. In (b) we also plot the SNR but now considering the cavity with a single-mode squeezed state with squeezing parameter $\theta = \pi/4$ and $r = 20$ (dB) $\equiv e^{2r} = 100$ and homodyne angle $\phi = \pi/4$ for a time $t_f = 30$ ns. The other system parameters for the calculation are the same as those in Fig. 2.

separation, we further define the relative separation $d = |\langle \hat{a}_{\text{out},e}(t) \rangle - \langle \hat{a}_{\text{out},g}(t) \rangle|$, where $\langle \hat{a}_{\text{out},\ell}(t) \rangle = \sqrt{\kappa} \langle \hat{a}(t) \rangle$ is the output field averaged with respect to the qubit states $|\ell\rangle = \{|e\rangle, |g\rangle\}$.

Figure 2 shows the dependence of relative separation d on t/t_f . Fig. 2 (a) demonstrates that the modulations designed from STA produce the pointer state separation that is ten times larger than the normal sinusoidal modulation in Ref. [26] at timescale $t_f = \pi/(100 \kappa) \approx 30$ ns, thus yielding a fast qubit readout. For completeness, we further compare in Fig. 2 (b) the performance of our designed modulations with polynomial and trigonometric ansatzes. Though at shorter time trigonometric modulation performs better than polynomial one, at final time t_f both modulations reach the same values, due to the fixed boundary condition (5). To compare their performance for different t_f we plot the quantity $F(\kappa, t_f) \equiv e^{-\kappa t_f/2} \int_0^{t_f} g_c(s) e^{\kappa s/2} ds$ for different κ and t_f . Notice that $F(\kappa, t_f)$ gives us the maximal cavity displacement at fixed κ and t_f , respectively. From Fig. 2 (b) and Fig. 2 (c), we observe both modulations start to behave similarly, as long as t approaches t_f . Actually, we can also check the fluctuation on the cavity in the final readout. Based on it, we cannot attribute the enhanced performance to different engineered pulses, which only depends on the final boundary conditions.

Moreover, distant pointer state permits us to perform high-fidelity qubit measurement quantified through the signal-to-noise ratio (SNR) corresponding to the ratio between the homodyne signal with its fluctuations. We define the signal as $|\langle \hat{\mathcal{M}}_e \rangle - \langle \hat{\mathcal{M}}_g \rangle|$ where $\langle \hat{\mathcal{M}}_k \rangle$ is the average of the homodyne operator $\hat{\mathcal{M}}(\tau) = \sqrt{\kappa} \int_0^\tau ds (a_{\text{out}}^\dagger(t) \exp(i\phi) + a_{\text{out}}(t) \exp(-i\phi))$ with respect to the qubit state, and we refer to fluctuations by $\sqrt{\langle \hat{\mathcal{M}}_{Ne}^2 \rangle + \langle \hat{\mathcal{M}}_{Ng}^2 \rangle}$ with $\hat{\mathcal{M}}_{N\ell} = \hat{\mathcal{M}}_\ell - \langle \hat{\mathcal{M}}_\ell \rangle$ as the noise homodyne operator. The SNR is then defined as

$$\text{SNR}(\kappa\tau) = \frac{|\langle \hat{\mathcal{M}}_e \rangle - \langle \hat{\mathcal{M}}_g \rangle|}{\sqrt{\langle \hat{\mathcal{M}}_{Ne}^2 \rangle + \langle \hat{\mathcal{M}}_{Ng}^2 \rangle}}. \quad (9)$$

In Fig. 3 (a), we plot the SNR as a function of the dimensionless integration time τ/t_f using the polynomial (red dashed) and trigonometric (orange dotted) modulations, see Eqs. (6) and (7), designed from inverse engineering approach. We see an enhancement in the SNR, achieving the values approximately ten times larger than the sinusoidal modulation proposed at the time scale t_f . Furthermore, at short measuring time $\kappa\tau \ll 1$ we obtain the asymptotic scaling of SNR as $\text{SNR}(\kappa\tau) \approx (\kappa\tau)^{9/4}$, which approves the enhancement in time on quantum nondemolition measurement. Our result agrees with the statement in Ref. [26] that the readout performance can be improved by quantum control methods.

Moreover, we obtain the further improvement of SNR by considering the LC oscillator prepared in a single-mode squeezed orthogonal to the field displacement. The squeezed state only modifies the noise homodyne operator as $\hat{\mathcal{M}}_{N\ell} = \kappa\tau (\cosh(2r) + \sinh(2r) \cosh(2(\phi - \theta)))$ [26], where r and θ are the squeeze parameters and ϕ is the homodyne angle. By choosing $\phi - \theta = \pi/2 \bmod \pi$, we finally achieve $\hat{\mathcal{M}}_{N\ell} = \kappa\tau \exp(-2r)$, that leads to the exponential improvement on the SNR illustrated in Fig. 3 (b).

IV. COMPARISON TO COUNTER-DIABATIC DRIVING

An alternative way to accelerate the qubit readout relies upon the counter-diabatic driving [30]. Similar to STA for Rabi model [37], the counter-diabatic term for the Hamiltonian in Eq. (1) is calculated as

$$\mathcal{H}_{\text{CD}} = -i \frac{\dot{g}_z(t)}{\omega_r} \sigma^z (a^\dagger - a). \quad (10)$$

This interaction could be implemented in cQED architecture with a tunable capacitive interaction [38], which has not been easily implemented yet. To circumvent this problem, we utilize the multiple Schrödinger/interaction pictures [39] and express the Hamiltonian $\mathcal{H} + \mathcal{H}_{\text{CD}}$ in a rotating frame, which has different structure, but the same underlying physics. By using $\mathcal{U}(t) = \exp(-i \int_0^t \tilde{g}_z(s) \sigma^z (a^\dagger + a) / \omega_r^2 ds)$, we arrive at the effective Hamiltonian $\tilde{\mathcal{H}} = \omega_q \sigma^z / 2 + \omega_r \hat{a}^\dagger \hat{a} + \tilde{g}_z(t) \sigma^z (\hat{a}^\dagger + \hat{a})$, where $\tilde{g}_z(t) = g_z(t) + \ddot{g}_z(t) / \omega_r^2$ is the effective longitudinal coupling. In this new frame, it only requires a new modulation on the coupling strength $\tilde{g}_z(t)$ rather than complicated implementation, for instance, in a current experiment on open cQED [33].

Moreover, such approximate counter-diabatic driving can be implemented by using Floquet engineering (FE) [40–43]. Here, we add a high-frequency driving with a complex time dependency to emulate the counter-diabatic term only using the operators available on the system Hamiltonian. In what follows we will calculate the FE Hamiltonian such that its dynamics corresponds to the same as \mathcal{H}_{CD} . Essentially, to obtain the state preparation, up to the phase factor, it is not necessary to include the original Hamiltonian \mathcal{H} . For doing so, we define the Floquet engineering Hamiltonian as follows:

$$\mathcal{H}_{\text{FE}}(t) = \Omega \nu \sin(\nu t) (\sigma^z + a^\dagger a) + \lambda(t) \sigma^z (a^\dagger + a), \quad (11)$$

where $\nu \ll \omega_r$ is an arbitrary frequency, and Ω is a free parameter. Next, we express \mathcal{H}_{FE} in the rotating frame described by the following unitary transformation

$$\hat{U}(t) = \exp \left[i\Omega \cos \nu t (\sigma^z + a^\dagger a) \right]. \quad (12)$$

In the rotating frame, the effective Hamiltonian $\tilde{\mathcal{H}}_{\text{FE}}(t) = \hat{U}^\dagger(t) \mathcal{H}_{\text{FE}} \hat{U}(t) - i\hat{U}^\dagger(t) \dot{\hat{U}}(t)$ reads

$$\tilde{\mathcal{H}}_{\text{FE}} = \lambda(t) \hat{U}^\dagger(t) \sigma^z (a^\dagger + a) \hat{U}(t). \quad (13)$$

Using the Baker-Campbell-Hausdorff formula, we express the transformed Hamiltonian as

$$\tilde{\mathcal{H}}_{\text{FE}}(t) = \lambda(t) \sigma^z (a^\dagger e^{-i\Omega \cos \nu t} + a e^{i\Omega \cos \nu t}). \quad (14)$$

We proceed by calculating the average of the Hamiltonian over the period $T = 2\pi/\nu$ to get the first term of the Magnus expansion

$$\tilde{\mathcal{H}}_{\text{FE}}^{(0)}(t) = \frac{1}{T} \int_0^T \lambda(t) \sigma^z (a^\dagger e^{-i\Omega \cos \nu t} + a e^{i\Omega \cos \nu t}) dt. \quad (15)$$

To obtain that $\tilde{\mathcal{H}}_{\text{FE}}^{(0)} = \mathcal{H}_{\text{CD}}$ we require that

$$\frac{1}{T} \int_0^T \lambda(t) e^{-i\Omega \cos \nu t} dt = -i \frac{\dot{g}_z(t)}{\omega_r}, \quad (16)$$

$$\frac{1}{T} \int_0^T \lambda(t) e^{i\Omega \cos \nu t} dt = i \frac{\dot{g}_z(t)}{\omega_r}. \quad (17)$$

We proceed by assuming that $\lambda(t) = \sum_n C_n \cos(n\nu t)$, and we define $\alpha = \nu t$. In this case, the integrals above defined read

$$\sum_n \frac{C_n}{\pi} \int_0^\pi \cos(n\alpha) e^{-i\Omega \cos \alpha} d\alpha = -i \frac{\dot{g}_z(t)}{\omega_r}. \quad (18)$$

Notice that this integral looks similar to the definition of the Bessel function

$$J_n(z) = \frac{i^{-n}}{\pi} \int_0^\pi e^{iz \cos \theta} \cos(n\theta) d\theta. \quad (19)$$

With this definition Eq. (16) and Eq. (17) read

$$\sum_n i^n C_n J_n(\Omega) = -i \frac{\dot{g}_z(t)}{\omega_r}, \quad (20)$$

$$\sum_n i^n C_n J_n(-\Omega) = i \frac{\dot{g}_z(t)}{\omega_r}. \quad (21)$$

These conditions are met when $n = 2m + 1, \forall m \in \mathbb{Z}$. Thus, for $n = 1$ we have $\lambda(t) = C_1 \cos(\nu t)$ leading to

$$C_1 = \frac{\dot{g}_z(t)}{\omega_r J_1(\Omega)}. \quad (22)$$

Finally, the Floquet engineered Hamiltonian takes the following form:

$$\mathcal{H}_{\text{FE}}(t) = \Omega \nu \sin(\nu t) (\sigma^z + a^\dagger a) + \frac{\dot{g}_z(t)}{\omega_r J_1(\Omega)} \cos(\nu t) \sigma^z (a^\dagger + a), \quad (23)$$

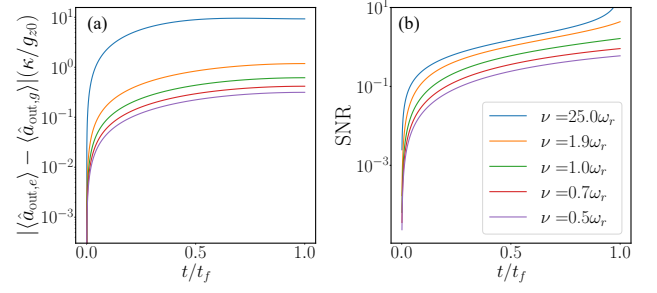


FIG. 4. (a) Relative pointer state separation for the output cavity field \hat{a}_{out} as function of t/t_f for different values of the frequency ν . (b) Signal-to-noise ratio (SNR) as function of the dimensionless measuring time τ/t_f . We have performed the simulation with the parameters $\kappa/2\pi = 1$ MHz, $g_{z0}/2\pi = 21$ MHz, $\omega_r/2\pi = 6.6$ GHz for $t_f = \pi/(100\kappa)$, and $\Omega = 1$.

where $\nu \ll \omega_r$ is an arbitrary frequency, Ω is a free parameter, and J_1 is the Bessel function of the first kind. By implementing the only Floquet Hamiltonian (not including the original Hamiltonian \mathcal{H}), we show the relative distance between the pointer states and the SNR can be significantly enhanced for different values of ν .

In Fig. 4, we show the relative distance between the pointer states and the signal-to-noise ratio (SNR) for the Floquet Hamiltonian in Eq. (23) for different values of ν . As expected by increasing the frequency on the modulation, larger pointer state separation we achieve leading to larger values of the SNR.

V. GENETIC ALGORITHM FOR OPTIMIZATION

Now, we turn to the genetic algorithm [44], an optimization subroutine based on the fundamentals of natural selection, in order to complement our inverse-engineering method. We formulate the optimization problem by assuming $g_c(t) = \sum_m c_m \cos(m\pi t/t_f) + d_m \sin(m\pi t/t_f)$, where the coefficients $\{c_m, d_m\}$ are to be optimized according the constrains provided by Eqs. (4a), (4b), and (5), respectively. Fig. 5 illustrates the design for g_z and corresponding SNR by fixing the number of coefficients. Surprisingly, the increase of the numbers of coefficients does not always lead to better SNR, as depicted in the inline of Fig. 5 (b), where the performance of the modulation with 8 coefficients surpasses that with 20. In this sense, the genetic algorithms provide a simpler but efficient modulation for achieving the same SNR at shorter time $t_f/2$. Of course, other optimization techniques, i.e., machine learning [45] and pulse shaping [16, 46] can be incorporated as well, since there exists the freedom left in inverse-engineering method mentioned above.

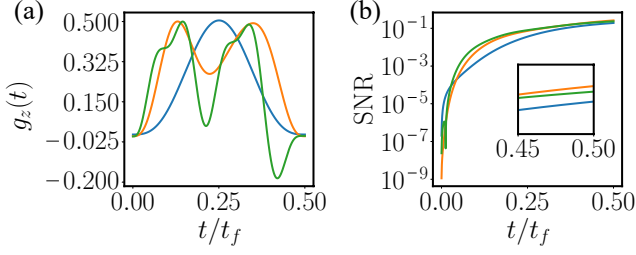


FIG. 5. (a) The modulation of coupling strength $g_z(t)$ optimized by the genetic algorithm containing 8 (blue), 12 (orange), and 20 (green) coefficients, respectively. (b) The corresponding SNR obtained with the genetic algorithm. We have performed the simulation with the same parameters as Fig. 2, except for the measuring time being $t_f/2$.

VI. PHYSICAL IMPLEMENTATION

A. Circuit Hamiltonian

We shall shed light on the experimental implementation for a two-level system coupled to an oscillator via longitudinal interaction. The circuit consist in an LC resonator of capacitance C_r and inductance L_r coupled to a transmon qubit [47] through a SQUID. The transmon qubit consists of a capacitor C_B parallel-connected Josephson junction of capacitance C_J and tunable Josephson energy $E_J(\phi_x)$. Moreover, we bias the circuit with an external gate voltage V_g connected to the transmon with the gate capacitance C_g . On the other hand, the SQUID is modeled as a tunable Josephson junction with effective capacitance C_{JS} , and Josephson energies $E_{JS}(\varphi_x)$. We write the Lagrangian of the circuit in terms of the flux nodes of each device $\{\psi_J, \psi_r\}$ related with the voltage drop across their respective branch $\psi_\ell = \int_{-\infty}^t V_\ell(x, t') dt'$ leading to

$$\begin{aligned} \mathcal{L}_c = & \frac{C_g}{2}(V_g - \dot{\psi}_J)^2 + \frac{C_T}{2}\dot{\psi}_J^2 + \frac{C_r}{2}\dot{\psi}_r^2 \\ & + \frac{C_S}{2}(\dot{\psi}_J - \dot{\psi}_r)^2 - \frac{\psi_r^2}{2L_r} + E_J(\phi_x) \cos\left(\frac{\psi_J}{\varphi_0}\right) \\ & + E_{JS}(\varphi_x) \cos\left(\frac{\psi_J - \psi_r}{\varphi_0}\right), \end{aligned} \quad (24)$$

where $\varphi_0 = \hbar/(2e)$ is the quantum magnetic flux and e is the electron charge. Besides, $C_T = C_B + C_J$ is the effective transmon capacitance. We calculate the canonical conjugate momenta $P_\ell = \partial\mathcal{L}_c/\partial[\dot{\psi}_\ell]$

$$P_J = (C_T + C_S + C_g)\dot{\psi}_J - C_S\dot{\psi}_r - C_gV_g, \quad (25)$$

$$P_r = (C_r + C_S)\dot{\psi}_r - C_S\dot{\psi}_J. \quad (26)$$

Here we have dropped the terms proportional to V_g^2 . In matrix form we have $\vec{P} = \hat{C} \vec{\Psi} - \vec{Q}_g$, where $\vec{P}^T = (P_J, P_r)$ and $\vec{\Psi}^T = (\psi_J, \psi_r)$ is the charge and flux vectors, respectively. Furthermore, $\vec{Q}_g^T = (C_gV_g, 0)$ is the gate charge vector, and

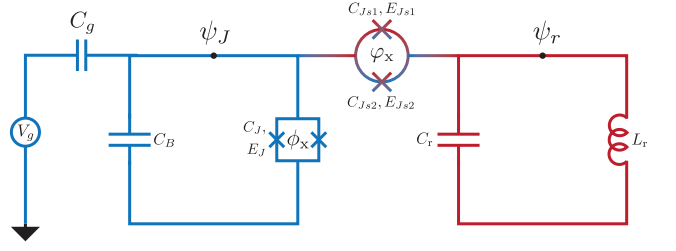


FIG. 6. Schematic illustration of the experimental proposal: a transmon qubit formed by a capacitor C_B parallel-connected to a tunable inductor is biased by a gate voltage V_g through a gate capacitor C_g , the two-level system coupled to an LC resonator of capacitance C_r and inductance L_r via an asymmetric SQUID threaded by an external magnetic flux φ_x . Furthermore, we describe the circuit in terms of their fluxes node ψ_J and ψ_r .

\hat{C} is the capacitance matrix

$$\hat{C} = \begin{pmatrix} C_\Sigma & -C_S \\ -C_S & C_\gamma \end{pmatrix}, \quad (27)$$

where $C_\Sigma = C_T + C_S + C_g$ and $C_\gamma = C_r + C_S$ are effective transmon and resonator capacitances, respectively. We obtain the circuit Hamiltonian through the Legendre transformation $\mathcal{H} = \vec{P}^T \vec{\Psi} - \mathcal{L}_c$ Where $\vec{\Psi} = \hat{C}^{-1}(\vec{P} + \vec{Q}_g)$ with \hat{C}^{-1} being the inverse of the capacitance matrix. The circuit Hamiltonian reads

$$\begin{aligned} \mathcal{H} = & \frac{C_\gamma P_J^2}{2(C_\Sigma C_\gamma - C_S^2)} + \frac{C_\Sigma P_r^2}{2(C_\Sigma C_\gamma - C_S^2)} + \frac{C_S P_J P_r}{(C_\Sigma C_\gamma - C_S^2)} \\ & + \frac{C_\gamma P_J Q_g}{(C_\Sigma C_\gamma - C_S^2)} + \frac{C_S P_r Q_g}{(C_\Sigma C_\gamma - C_S^2)} + \frac{\psi_r^2}{2L_r} \\ & - E_J(\phi_x) \cos\left(\frac{\psi_J}{\varphi_0}\right) - E_{JS}(\varphi_x) \cos\left(\frac{\psi_J - \psi_r}{\varphi_0}\right). \end{aligned} \quad (28)$$

To proceed, we assume that the SQUID works on a parameter regime where the capacitive interaction is smaller than the Josephson energy, regarding only inductive interaction between the subsystems [24–27]. Thus, for small C_S we neglect the capacitive interaction and we rewrite the potential energy obtaining

$$\begin{aligned} \mathcal{H} = & \frac{C_\gamma P_J^2}{2(C_\Sigma C_\gamma - C_S^2)} + \frac{C_\Sigma P_r^2}{2(C_\Sigma C_\gamma - C_S^2)} + \frac{C_\gamma P_J Q_g}{(C_\Sigma C_\gamma - C_S^2)} \\ & + \frac{\psi_r^2}{2L_r} - E_J(\phi_x) \cos\left(\frac{\psi_J}{\varphi_0}\right) \\ & - E_{JS}(\varphi_x) \cos\left(\frac{\psi_J - \psi_r}{\varphi_0}\right). \end{aligned} \quad (29)$$

We now assume that the SQUID works in the linear regime [57] meaning that the mostly of the current flows through the transmon. Hence, the resonator phase is well locate allowing to expand the potential energy up to its leading

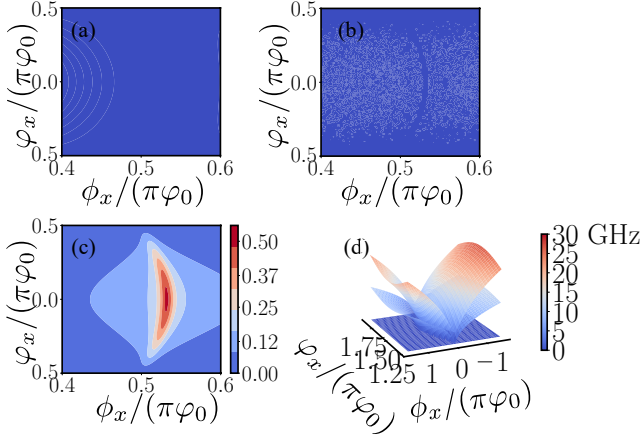


FIG. 7. (a)-(c) Pauli matrix coefficient $\alpha_k = \text{Tr}[\sigma^k \cos(\hat{\theta}_J)]$ for the coupling operator as a function of the external magnetic fluxes ϕ_x and φ_x . (d) Low-lying energy spectrum of the transmon Hamiltonian \mathcal{H}_T as a function of the external magnetic fluxes ϕ_x and φ_x . We have performed the simulation choosing the parameters $E_J/\hbar = 2\pi \times 20$ GHz, $E_C = E_J/67$, $E_S/\hbar = 2\pi \times 30$ GHz $\equiv 1.5 E_J$, yielding $\omega_q = 2\pi \times 3.28$ GHz and $n_g = 0.5$.

order in ψ_r/φ_0 [58]

$$\begin{aligned} \mathcal{H} &= \frac{C_\gamma P_J^2}{2(C_\Sigma C_\gamma - C_S^2)} + \frac{C_\Sigma P_r^2}{2(C_\Sigma C_\gamma - C_S^2)} + \frac{C_\gamma P_J Q_g}{(C_\Sigma C_\gamma - C_S^2)} \\ &- E_J(\phi_x) \cos\left(\frac{\psi_J}{\varphi_0}\right) - E_{JS}(\varphi_x) \cos\left(\frac{\psi_J}{\varphi_0}\right) + \frac{\psi_r^2}{2L_r} \\ &- E_{JS}(\varphi_x) \cos\left(\frac{\psi_J}{\varphi_0}\right) \psi_r. \end{aligned} \quad (30)$$

We proceed to quantize the circuit Hamiltonian by promoting the classical variables to quantum operators. For the transmon qubit the charge of the circuit is proportional to the number of Cooper-pair $P_J \rightarrow -2e\hat{n}_J$ and its conjugate variable corresponds to the phase drop $\hat{\theta}_J = \psi_J/\varphi_0$ satisfying commutation relation $[\hat{P}_J, e^{i\hat{\theta}_J}] = i$. For the LC resonator, the operators satisfies $[\hat{\psi}_J, \hat{P}_J] = i\hbar$. The quantum circuit Hamiltonian reads

$$\begin{aligned} \mathcal{H} &= E_C(\hat{n}_J - n_g)^2 - E_{\hat{J}}(\phi_x, \varphi_x) \cos(\hat{\theta}_J) \\ &+ \hbar\omega_r \hat{a}^\dagger \hat{a} - \frac{E_{JS}(\varphi_x)}{\varphi_0} \sqrt{\frac{\hbar\omega_r L_r}{2}} (\hat{a}^\dagger + \hat{a}) \cos(\hat{\theta}_J). \end{aligned} \quad (31)$$

Here, $E_C = 2e^2 C_\gamma / (C_\Sigma C_\gamma - C_S^2)$ and $E_{\hat{J}}(\phi_x, \varphi_x) = E_J(\phi_x) + E_{JS}(\varphi_x)$ correspond to the charge energy and the effective Josephson energy of the transmon, respectively, $n_g = Q_g/2e^2$ stands for the dimensionless gate charge. Besides, $\omega_r = \sqrt{C_\Sigma / ((C_\Sigma C_\gamma - C_S^2) L_r)}$ is the oscillator frequency. It is convenient to divide the circuit Hamiltonian in

three parts

$$\mathcal{H}_T = E_C(\hat{n}_J - n_g)^2 - E_{\hat{J}}(\phi_x, \varphi_x) \cos(\hat{\theta}_J), \quad (32)$$

$$\mathcal{H}_r = \hbar\omega_r \hat{a}^\dagger \hat{a}, \quad (33)$$

$$\mathcal{H}_I = -\frac{E_{JS}(\varphi_x)}{\varphi_0} \sqrt{\frac{\hbar\omega_r L_r}{2}} (\hat{a}^\dagger + \hat{a}) \cos(\hat{\theta}_J), \quad (34)$$

corresponding to the transmon, resonator and interaction Hamiltonian respectively.

B. Two-level approximation

Next, we turn to illustrate that in the two-level approximation of the transmon qubit, the Hamiltonian \mathcal{H}_I leads to a longitudinal oscillator qubit interaction. We express this Hamiltonian in the charge basis $|n_J\rangle$ choosing $|g\rangle \equiv |0\rangle$ and $|e\rangle \equiv |1\rangle$ the Hamiltonian reads (up to terms proportional to n_g^2)

$$\mathcal{H}_T = E_C(1 - 2n_g)|e\rangle\langle e| - \frac{E_{\hat{J}}(\phi_x, \varphi_x)}{2} \sigma^x, \quad (35)$$

$$\mathcal{H}_I = -\frac{E_{JS}(\varphi_x)}{2\varphi_0} \sqrt{\frac{\hbar\omega_r L_r}{2}} (\hat{a}^\dagger + \hat{a}) \sigma^x, \quad (36)$$

where $\sigma^x = |1\rangle\langle 0| + |0\rangle\langle 1|$. For an external gate charge $n_g = 0.5$ we obtain that the first term of \mathcal{H}_T vanishes. Then it is possible to write as follows

$$\mathcal{H}_T = \frac{\hbar\omega_q(\phi_x, \varphi_x)}{2} \sigma^z, \quad (37)$$

where $\omega_q = \sqrt{E_{\hat{J}}^2(\phi_x, \varphi_x)/\hbar}$ is the transition frequency of the qubit. Similar to the coupling operator. To prove that, In Fig. 7, we have calculated the coefficients $\alpha_k = \text{Tr}[\sigma^k \cos(\hat{\theta}_J)]$ writing the operator $\cos(\hat{\theta}_J)$ in the diagonal basis of \mathcal{H}_T observing that there is no contributions of either σ^x or σ^y . Therefore, the interaction Hamiltonian can be expressed as follows

$$\mathcal{H}_I = -\frac{E_{JS}(\varphi_x)}{2\varphi_0} \sqrt{\frac{\hbar\omega_r L_r}{2}} (\hat{a}^\dagger + \hat{a}) \sigma^z. \quad (38)$$

Finally, the circuit Hamiltonian reads

$$\mathcal{H} = \hbar\omega_r \hat{a}^\dagger \hat{a} + \frac{\hbar\omega_q}{2} \sigma^z + \hbar g_z(t) (\hat{a}^\dagger + \hat{a}) \sigma^z, \quad (39)$$

$$g_z(t) = \frac{\omega_q}{2\varphi_0} \sqrt{\frac{\hbar\omega_r L_r}{2}}. \quad (40)$$

In Fig. 7 we have also plot the energy spectrum of the transmon Hamiltonian as function of both external magnetic fluxes ϕ_x and φ_x . We see that the energy spectrum of the two-level system does not exhibit abrupt changes along φ_x corresponding to the tunable coupling strength. Consequently, it is possible to switch the coupling strength without modifying the energy spectrum of the qubit.

C. Estimation of the coupling strength and minimal time

From the last subsection, we have obtained that under suitable conditions the circuit corresponds to a qubit longitudinally coupled to an oscillator with coupling strength given by

$$g_z(t) = \frac{\omega_q}{2\varphi_0} \sqrt{\frac{\hbar\omega_r L_r}{2}}. \quad (41)$$

From this expression we observe that the coupling strength depends mainly on four parameters, the qubit frequency, the sum of the Josephson energy of the SQUID, and the resonator capacitance and inductance. Thus considering consistent cQED values it is possible to estimate the maximal value of $g_z(t)$. To achieve larger values of the coupling strength that yields to faster measuring time we require large impedance [59]. In this direction, technological progress has made possible to engineer inductances in the μH regime using arrays of Josephson junctions or taking into account kinetic inductors [49–52]. To estimate the value of the coupling strength we regard $\phi_x/\varphi_0 = \varphi_x/\varphi_0 = \pi/4$, hence the qubit frequency turns into $\omega_q = \sqrt{E_C^2 + dE_\Sigma^2}/\hbar$. For realistic cQED parameters $E_J/\hbar = 2\pi \times 20$ GHz, $E_C = E_J/67$ [26], $E_\Sigma/\hbar = 2\pi \times 30$ GHz $\equiv 1.5 E_J$ [53] and $d = 0.02$ we obtain $\omega_q = 2\pi \times 3.28$ GHz. Moreover, for an LC oscillator (or transmission line resonator) having values $\omega_r L_r = 200$ k Ω [49] we achieve $g_z(t) = 2\pi \times 2.57$ GHz corresponding to $\max(g_z)/\omega_r \equiv 0.5793$.

With this maximal value, it is possible to estimate the minimal time required to measure the qubit $t_{\min} = \pi/(2\omega_r)$, on a subnanosecond time scale, from optimal control theory, see the detailed discussion in Appendix B.

VII. CONCLUSION

In summary, the methods of STA, including inverse engineering and counter-diabaticity, have been worked out for designing the longitudinal qubit-cavity coupling to accelerate the qubit measurement. Remarkably, by engineering the modulations, the pointer state separation is significantly enhanced, accompanied by a large SNR. We also see an exponential enhancement when the cavity in a single-mode is prepared in squeezed state. In addition, genetic algorithm are discussed also for the optimization. In the cQED platform, tunable capacitive interaction is required to implement counter-diabatic driving, which makes the inverse-engineering approach more feasible to speed up the measurement process, with the realistic cQED architecture. We estimate an upper bound for the coupling strength that set the low bound for measuring time. Last but not least, we hope our result can be experimentally verified with circuit design implementing longitudinal coupling of superconducting qubits [26, 54], and applicable to electronic spin readout as well [55, 56].

ACKNOWLEDGMENTS

This work is partially supported from NSFC (12075145), STCSM (2019SHZDZX01-ZX04), QMiCS (820505) and OpenSuperQ (820363) of the EU Flagship on Quantum Technologies, EU FET Open Grant Quomorphic (828826) and EPIQUS (899368), QUANTEK project (KK-2021/00070), and the Basque Government through Grant No. IT1470-22. X.C. acknowledges the Ramón y Cajal program (RYC-2017-22482).

Appendix A: Elimination of the longitudinal coupling

Let us consider a two-level system longitudinally coupled to an oscillator described by the Hamiltonian Eq. (1), where ω_q is the transition frequency of the qubit, ω_r is the oscillator frequency. Furthermore, σ^z is the z -component Pauli matrix describing the two-level system, and a^\dagger (a) is the creation (annihilation) operator of the oscillator. We will show that the unitary transformation

$$\mathcal{V}(t) = e^{i\theta(t)} e^{-i\frac{\dot{g}_c(t)\sigma^z(a^\dagger+a)}{\omega_r^2}} e^{-\frac{g_c(t)}{\omega_r}\sigma^z(a^\dagger-a)},$$

presented in the manuscript eliminates the longitudinal coupling strength leading to the effective Hamiltonian $\mathcal{H}_{\text{eff}} = \mathcal{V}^\dagger \mathcal{H} \mathcal{V} - i\mathcal{V}\dot{\mathcal{V}}^\dagger \equiv \omega_r a^\dagger a + \omega_q \sigma^z/2$. Here, $\theta(t)$ corresponds to a phase defined as

$$\theta(t) = -\int_0^t \mathcal{L}_g(t') dt, \quad (A1)$$

where \mathcal{L}_g is a Lagrangian that relates the quantities $g_z(t)$ and $g_c(t)$ through the following relation:

$$\mathcal{L}_g(t) = \frac{\dot{g}_c^2(t)}{\omega_r^3} - \frac{g_c^2(t)}{\omega_r} + \frac{2g_c(t)g_z(t)}{\omega_r}. \quad (A2)$$

For this derivation it is convenient to divide in three the effective Hamiltonian in three terms regarding the free terms ($\mathcal{H}_{\text{eff},1}$), the transformed longitudinal interaction ($\mathcal{H}_{\text{eff},2}$) and the terms appearing due the transformation $\mathcal{H}_{\text{eff},3} = -i\mathcal{V}\dot{\mathcal{V}}^\dagger$. For the free terms we obtain

$$\begin{aligned} \mathcal{H}_{\text{eff},1} &= \mathcal{V}^\dagger \left(\frac{\omega_q}{2} \sigma^z + \omega_r \hat{a}^\dagger \hat{a} \right) \mathcal{V} \\ &= \frac{\omega_q}{2} \sigma^z + \omega_r \hat{a}^\dagger \hat{a} + \frac{i\dot{g}_c(t)}{\omega_r} \sigma^z [\hat{a}^\dagger + \hat{a}, \hat{a}^\dagger \hat{a}] \\ &\quad + g_c(t) \sigma^z [\hat{a}^\dagger - \hat{a}, \hat{a}^\dagger \hat{a}] - \frac{\dot{g}_c^2(t)}{2\omega_r^3} [\hat{a}^\dagger + \hat{a}, [\hat{a}^\dagger + \hat{a}, \hat{a}^\dagger \hat{a}]] \\ &\quad + \frac{i\dot{g}_c(t)g_c(t)}{2\omega_r^2} [\hat{a}^\dagger + \hat{a}, [\hat{a}^\dagger - \hat{a}, \hat{a}^\dagger \hat{a}]] \\ &\quad + \frac{i\dot{g}_c(t)g_c(t)}{2\omega_r^2} [\hat{a}^\dagger - \hat{a}, [\hat{a}^\dagger + \hat{a}, \hat{a}^\dagger \hat{a}]] \\ &\quad + \frac{g_c^2(t)}{2\omega_r} [\hat{a}^\dagger - \hat{a}, [\hat{a}^\dagger - \hat{a}, \hat{a}^\dagger \hat{a}]]. \end{aligned} \quad (A3)$$

In this derivation, we have used the Baker-Campbell-Hausdorff formulae keeping terms up to second order in the

coupling strength g_c and \dot{g}_c , respectively. After solving the commutators we arrive at

$$\begin{aligned} \mathcal{H}_{\text{eff},1} = & \frac{\omega_q}{2} \sigma^z + \omega_r \hat{a}^\dagger \hat{a} \\ & - \frac{i\dot{g}_c(t)}{\omega_r} \sigma^z (\hat{a}^\dagger - \hat{a}) - g_c(t) \sigma^z (\hat{a}^\dagger + \hat{a}) \\ & + \frac{\dot{g}_c^2(t)}{\omega_r^3} + \frac{g_c^2(t)}{\omega_r}. \end{aligned} \quad (\text{A4})$$

With the same procedure we obtain the transformed longitudinal coupling $\mathcal{H}_{\text{eff},2}$ as follows

$$\mathcal{H}_{\text{eff},2} = g_z(t) \sigma^z (\hat{a}^\dagger + \hat{a}) - \frac{2g_c(t)g_z(t)}{\omega_r}. \quad (\text{A5})$$

Similar for $\mathcal{H}_{\text{eff},3}$ we obtain

$$\begin{aligned} \mathcal{H}_{\text{eff},3} = & -\dot{\theta}(t) + \frac{\ddot{g}_c(t)}{\omega_r^2} \sigma^z (\hat{a}^\dagger + \hat{a}) \\ & + \frac{i\dot{g}_c(t)}{\omega_r} \sigma^z (\hat{a}^\dagger - \hat{a}) - \frac{2\dot{g}_c^2(t)}{\omega_r^3}. \end{aligned} \quad (\text{A6})$$

Finally, we arrive at the effective Hamiltonian

$$\begin{aligned} \mathcal{H}_{\text{eff}} = & \frac{\omega_q}{2} \sigma^z + \omega_r \hat{a}^\dagger \hat{a} - \dot{\theta}(t) \\ & + \left[\frac{\ddot{g}_c(t)}{\omega_r^2} - g_c(t) + g_z(t) \right] \sigma^z (\hat{a}^\dagger + \hat{a}) \\ & - \left[\frac{\dot{g}_c^2(t)}{\omega_r^3} - \frac{g_c^2(t)}{\omega_r} + \frac{2g_c(t)g_z(t)}{\omega_r} \right]. \end{aligned} \quad (\text{A7})$$

From the effective Hamiltonian in Eq. (A7) we see that for achieve $\mathcal{H}_{\text{eff}} = \mathcal{V}^\dagger \mathcal{H} \mathcal{V} - i\dot{\mathcal{V}} \mathcal{V}^\dagger \equiv \omega_r \hat{a}^\dagger \hat{a} + \omega_q \sigma^z / 2$, we require satisfy two conditions;

$$\dot{\theta}(t) = \frac{\dot{g}_c^2(t)}{\omega_r^3} - \frac{g_c^2(t)}{\omega_r} + \frac{2g_c(t)g_z(t)}{\omega_r}, \quad (\text{A8})$$

$$\ddot{g}_c(t) + \omega_r^2 [g_c(t) - g_z(t)] = 0. \quad (\text{A9})$$

Notice that Eq. (A8) is exactly the same as the Lagrangian in Eq. (A2), and the condition Eq. (A9) is nothing but the Euler-Lagrange equation for the Lagrangian \mathcal{L}_g . Thus, we concluded that the unitary transformation $\mathcal{V}(t)$ permit to us to express the system Hamiltonian \mathcal{H} , see Eq. (1), in a frame without longitudinal coupling strength.

Appendix B: Time-optimal control

Given the freedom left in reverse engineering based on Eq. (3), we combine it with optimal control theory (OCT) to find the minimal time for measurement according to the maximal coupling strength obtained above. In order to account for boundary conditions, we first enlarge the control system as

$g_d = \dot{g}_c$. The state of the system $X = (g_c, g_d)^\top$ satisfies the following differential system:

$$\dot{X} = AX + uB, \quad (\text{B1})$$

with the control $u = g_z$ and the matrices A and B defined as follows:

$$A = \begin{pmatrix} 0 & 1 \\ -\omega_r^2 & 0 \end{pmatrix} \text{ and } B = \begin{pmatrix} 0 \\ \omega_r^2 \end{pmatrix}. \quad (\text{B2})$$

We reformulate Eq. (3) into time-optimal control problem, by defining dynamical equations

$$\dot{g}_c = g_d, \quad (\text{B3})$$

$$\dot{g}_d = -\omega_r^2 (g_c - u). \quad (\text{B4})$$

To minimize the time $J = \int_0^{t_f} dt$, we apply the Pontryagin maximum principle to find the control $\{u, X(t)\}$ under the constraint $0 \leq u \leq u_m$ ($u_m = \max(g_z)$), consistent with the boundary conditions. The optimal control Hamiltonian is $H_c = p_0 + p_g g_d + p_d \omega_r^2 (u - g_c)$, with p_0 being the constant and (p_g, p_d) being the multipliers. The Pontryagin maximum principle tells [60] us that the adjoint state is the solution of the following differential equations,

$$\dot{p}_g = \omega_r p_d, \quad (\text{B5})$$

$$\dot{p}_d = -p_g, \quad (\text{B6})$$

from which the adjoint equations can be obtained as

$$p_d(t) = A_d \cos(\omega_r t) + B_d \sin(\omega_r t), \quad (\text{B7})$$

where A_d and B_d can be fixed by initial values $p_d(0)$. We can also introduce the switching function $\Phi = p_d$, such that

$$u = \begin{cases} \max(g_z), & \Phi > 0 \\ 0, & \Phi < 0 \end{cases}, \quad (\text{B8})$$

In the singular case we have $p_d = p_g = 0$ on a non-zero time interval, and this extremal cannot be reached since p_d, p_g are continuous. When $u = 0$, we have $\ddot{g}_c + \omega_r^2 g_c = 0$, yielding

$$g_c(t) = A_0 \cos(\omega_r t) + B_0 \sin(\omega_r t), \quad (\text{B9})$$

$$g_d(t) = -A_0 \omega_r \sin(\omega_r t) + B_0 \omega_r \cos(\omega_r t), \quad (\text{B10})$$

where A_0 and B_0 are constants determined later by boundary conditions. From this, we deduce that g_d and g_c cannot be simultaneously equal to zero at initial or final times, so $u = 0$ does not correspond to the first or last bang. However, we can still estimate the minimal time when $u = u_m$ on $[0, t_f]$. Therefore, from the initial boundary condition, we obtain:

$$g_c(t) = u_m (1 - \cos(\omega_r t)), \quad (\text{B11})$$

$$g_d(t) = \omega_r u_m \sin(\omega_r t). \quad (\text{B12})$$

We can notice that $\omega_r t_f = 2k\pi$ ($k = 1, 2, 3, \dots$), which gives the minimal measurement time $t_{\min} = \pi / (2\omega_r)$ ($k = 1$), which is on the subnanosecond time scale with the system parameters used here. Of course, one may consider other optimal problems with various constraints as well.

- [1] M. H. Devoret, J. M. Martinis, Implementing Qubits with Superconducting Integrated Circuits, *Experimental Aspects of Quantum Computing*, Springer, Boston, MA (2005).
- [2] J. Q. You, F. Nori, Superconducting Circuits and Quantum Information, *Phys. Today* **58**, 42 (2005).
- [3] J. Clarke and F. K. Wilhelm, Superconducting quantum bits, *Nature* **453**, 1031 (2008).
- [4] G. Wendin, and V.S. Shumeiko, Superconducting Quantum Circuits, Qubits and Computing, [arXiv:cond-mat/0508729](https://arxiv.org/abs/cond-mat/0508729) [**cond-mat.supr-con**] (2005).
- [5] M. H. Devoret, and R. J. Schoelkopf, Superconducting Circuits for Quantum Information: An Outlook, *Science*, **339**, 1169 (2013).
- [6] A. F. Kockum, and F. Nori, Quantum Bits with Josephson Junctions, *Fundamentals and Frontiers of the Josephson Effect*, Springer Series in Materials Science, Vol 286. Springer, Cham. (2019).
- [7] P. Krantz, M. Kjaergaard, F. Yan, T. P. Orlando, S. Gustavsson, W. D. Oliver, A Quantum Engineer's Guide to Superconducting Qubits, *Applied Physics Reviews* **6**, 021318 (2019).
- [8] M. Kjaergaard, M. E. Schwartz, J. Braumüller, P. Krantz, J. I. J. Wang, S. Gustavsson, and W. D. Oliver, Superconducting qubits: Current state of play, *Annual Review of Condensed Matter Physics*, **11**, 369 (2020).
- [9] J. M. Martinis, M. H. Devoret, and J. Clarke, Quantum Josephson junction circuits and the dawn of artificial atoms, *Nature Physics* **16**, 234 (2020).
- [10] A. Blais, R.-S. Huang, A. Wallraff, S. M. Girvin, and R. J. Schoelkopf, Cavity quantum electrodynamics for superconducting electrical circuits: An architecture for quantum computation, *Phys. Rev. A* **69**, 062320 (2004).
- [11] A. Wallraff, D. I. Schuster, A. Blais, L. Frunzio, R.-S. Huang, J. Majer, S. Kumar, S. M. Girvin, and R. J. Schoelkopf, Strong coupling of a single photon to a superconducting qubit using circuit quantum electrodynamics, *Nature* **431**, 162 (2004).
- [12] I. Chiorescu, P. Bertet, K. Semba, Y. Nakamura, C. J. P. M. Harmans, and J. E. Mooij, Coherent dynamics of a flux qubit coupled to a harmonic oscillator, *Nature* **431**, 159 (2004).
- [13] R. J. Schoelkopf and S. M. Girvin, Wiring up quantum systems, *Nature* **451**, 664 (2008).
- [14] A. Blais, A. L. Grimsmo, S. M. Girvin, and, A. Wallraff, Circuit quantum electrodynamics, *Rev. Mod. Phys.* **93**, 025005 (2021).
- [15] A. Blais, S. M. Girvin, and W. D. Oliver, Quantum information processing and quantum optics with circuit quantum electrodynamics, *Nature Physics* **16**, 247 (2020).
- [16] E. Jeffrey, D. Sank, J. Y. Mutus, T. C. White, J. Kelly, R. Barends, Y. Chen, Z. Chen, B. Chiaro, A. Dunsworth, A. Megrant, P. J. J. O'Malley, C. Neill, P. Roushan, A. Vainsencher, J. Wenner, A. N. Cleland, and J. M. Martinis, Fast Accurate State Measurement with Superconducting Qubits, *Phys. Rev. Lett.* **112**, 190504 (2014).
- [17] A. Wallraff, D. I. Schuster, A. Blais, L. Frunzio, J. Majer, M. H. Devoret, S. M. Girvin, and R. J. Schoelkopf, Approaching Unit Visibility for Control of a Superconducting Qubit with Dispersive Readout, *Phys. Rev. Lett.* **95**, 060501 (2005).
- [18] F. Mallet, F. R. Ong, A. Palacios-Laloy, F. Nguyen, P. Bertet, D. Vion, and D. Esteve, Single-shot qubit readout in circuit quantum electrodynamics, *Nature Physics* **5**, 791(2009).
- [19] L. Tornberg and G. Johansson, High-fidelity feedback-assisted parity measurement in circuit QED, *Phys. Rev. A* **82**, 012329 (2010).
- [20] F. Motzoi, L. Buchmann, C. Dickel, Simple, smooth and fast pulses for dispersive measurements in cavities and quantum networks, [arXiv:1809.04116v1](https://arxiv.org/abs/1809.04116v1) [**quant-ph**] (2018).
- [21] A. A. Houck, J. A. Schreier, B. R. Johnson, J. M. Chow, Jens Koch, J. M. Gambetta, D. I. Schuster, L. Frunzio, M. H. Devoret, S. M. Girvin, and R. J. Schoelkopf, Controlling the Spontaneous Emission of a Superconducting Transmon Qubit, *Phys. Rev. Lett.* **101**, 080502 (2008).
- [22] M. Boissonneault, J. M. Gambetta, and A. Blais, Dispersive regime of circuit QED: Photon-dependent qubit dephasing and relaxation rates, *Phys. Rev. A* **79**, 013819 (2009).
- [23] D. H. Slichter, R. Vijay, S. J. Weber, S. Boutin, M. Boissonneault, J. M. Gambetta, A. Blais, and I. Siddiqi, Measurement-Induced Qubit State Mixing in Circuit QED from Up-Converted Dephasing Noise, *Phys. Rev. Lett.* **109**, 153601 (2012).
- [24] J. Bourassa, J. M. Gambetta, A. A. Abdumalikov, Jr., O. Astafiev, Y. Nakamura, and A. Blais, Ultrastrong coupling regime of cavity QED with phase-biased flux qubits, *Phys. Rev. A* **80**, 032109 (2009).
- [25] P.-M. Billangeon, J. S. Tsai, and Y. Nakamura, Circuit-QED-based scalable architectures for quantum information processing with superconducting qubits, *Phys. Rev. B* **91**, 094517 (2015).
- [26] N. Didier, J. Bourassa, and A. Blais, Fast Quantum Nondemolition Readout by Parametric Modulation of Longitudinal Qubit-Oscillator Interaction, *Phys. Rev. Lett.* **115**, 203601 (2015).
- [27] D. Kafri, C. Quintana, Y. Chen, A. Shabani, J. M. Martinis, and H. Neven, Tunable inductive coupling of superconducting qubits in the strongly nonlinear regime, *Phys. Rev. A* **95**, 052333 (2017).
- [28] Y. Zhou, Z. Zhang, Z. Yin, S. Huai, X. Gu, X. Xu, J. Allcock, F. Liu, G. Xi, Q. Yu, H. Zhang, M. Zhang, H. Li, X. Song, Z. Wang, D. Zheng, S. An, Y. Zheng, S. Zhang, Rapid and Unconditional Parametric Reset Protocol for Tunable Superconducting Qubits, *Nat. Comm.* **12**, 5924 (2021).
- [29] Xi. Chen, A. Ruschhaupt, S. Schmidt, A. del Campo, D. Guéry-Odelin, and J. G. Muga, Fast Optimal Frictionless Atom Cooling in Harmonic Traps: Shortcut to Adiabaticity, *Phys. Rev. Lett.* **104**, 063002 (2010).
- [30] D. Guéry-Odelin, A. Ruschhaupt, A. Kiely, E. Torrontegui, S. Martínez-Garaot, and J. G. Muga, Shortcuts to adiabaticity: Concepts, methods, and applications, *Rev. Mod. Phys.* **91**, 045001 (2019).
- [31] R. Dann, A. Tobalina, and R. Kosloff, Shortcut to Equilibration of an Open Quantum System, *Phys. Rev. Lett.* **122**, 250402 (2019).
- [32] S. Alipour, A. Chenu, A. T. Rezakhani, and A. del Campo, Shortcuts to Adiabaticity in Driven Open Quantum Systems: Balanced Gain and Loss and Non-Markovian Evolution, *Quantum* **4**, 336 (2020).
- [33] Zelong Yin, Chunzhen Li, Jonathan Allcock, Yicong Zheng, Xiu Gu, Maochun Dai, Shengyu Zhang, Shuoming An, Shortcuts to Adiabaticity for Open Systems in Circuit Quantum Electrodynamics, *Nat. Commun.* **13**, 188 (2022).
- [34] T. Čadež, J. H. Jefferson, and A. Ramšak, Exact Nonadiabatic Holonomic Transformations of Spin-Orbit Qubits, *Phys. Rev. Lett.* **112**, 150402 (2014).
- [35] X. Chen, R.-L. Jiang, J. Li, Y. Ban, and E. Ya. Sherman, Inverse engineering for fast transport and spin control of spin-orbit-coupled Bose-Einstein condensates in moving harmonic traps, *Phys. Rev. A* **97**, 013631 (2018).

- [36] C. Gardiner and P. Zoller, *Quantum Noise*, 3rd ed. (Springer, New York, 2004).
- [37] Y.-H. Chen, W. Qin, X. Wang, A. Miranowicz, and F. Nori, Shortcuts to Adiabaticity for the Quantum Rabi Model: Efficient Generation of Giant Entangled Cat States via Parametric Amplification, *Phys. Rev. Lett.* **126**, 023602 (2021).
- [38] G.-D. Yu, H.-O. Li, G. Cao, M. Xiao, H.-W. Jiang, and G.-P. Guo, Tunable capacitive coupling between two semiconductor charge qubits, *Nanotechnology* **27**, 324003 (2016).
- [39] S. Ibáñez, Xi Chen, E. Torrontegui, J. G. Muga, and A. Ruschhaupt, Multiple Schrödinger Pictures and Dynamics in Shortcuts to Adiabaticity, *Phys. Rev. Lett.* **109**, 100403 (2012).
- [40] D. Sels and A. Polkovnikov, Minimizing irreversible losses in quantum systems by local counterdiabatic driving, *Proceedings of the National Academy of Sciences* **114**, E3909 (2017).
- [41] P. W. Claeys, M. Pandey, D. Sels, and A. Polkovnikov, Floquet-Engineering Counterdiabatic Protocols in Quantum Many-Body Systems, *Phys. Rev. Lett.* **123**, 090602 (2019).
- [42] G. Passarelli, V. Cataudella, R. Fazio, and P. Lucignano, Counterdiabatic driving in the quantum annealing of the p-spin model: A variational approach, *Phys. Rev. Research* **2**, 013283 (2020).
- [43] L. Prielinger, A. Hartmann, Y. Yamashiro, K. Nishimura, W. Lechner, and H. Nishimori, Two-parameter counter-diabatic driving in quantum annealing, *Phys. Rev. Research* **3**, 013227 (2021).
- [44] W. Lee, H. Y. Kim, Genetic algorithm implementation in Python, *IEEE, ICIS'05*, 8 (2005).
- [45] E. Magesan, J. M. Gambetta, A. D. Córcoles, J. M. Chow, Machine learning for discriminating quantum measurement trajectories and improving readout. *Phys. Rev. Lett.* **114**, 200501 (2015).
- [46] D. T. McClure, H. Paik, L. S. Bishop, M. Steffen, Jerry M. Chow, and Jay M. Gambetta, Rapid Driven Reset of a Qubit Readout Resonator, *Phys. Rev. Applied* **5**, 011001(R) (2016).
- [47] J Koch, T. M. Yu, J. Gambetta, A. A. Houck, D. I. Schuster, J. Majer, A. Blais, M. H. Devoret, S. M. Girvin, R. J. Schoelkopf, Charge insensitive qubit design derived from the Cooper pair box, *Phys. Rev. A* **76**, 042319 (2007).
- [48] N. Samkharadze, A. Bruno, P. Scarlino, G. Zheng, D. P. DiVincenzo, L. DiCarlo, and L. M. K. Vandersypen, High-Kinetic-Inductance Superconducting Nanowire Resonators for Circuit QED in a Magnetic Field, *Phys. Rev. Applied* **5**, 044004 (2016).
- [49] I. V. Pechenezhskiy, R. A. Mencia, L. B. Nguyen, Y.-Hsiang Lin, and V. E. Manucharyan, The superconducting quasicharge qubit, *Nature* **585**, 368 (2020).
- [50] C. K. Andersen and A. Blais, Ultrastrong coupling dynamics with a transmon qubit, *New J. Phys.* **19**, 023022 (2016).
- [51] A. Stockklauser, P. Scarlino, J. V. Koski, S. Gasparinetti, C. K. Andersen, C. Reichl, W. Wegscheider, T. Ihn, K. Ensslin, A. Wallraff, Strong Coupling Cavity QED with Gate-Defined Double Quantum Dots Enabled by a High Impedance Resonator, *Phys. Rev. X* **7**, 011030 (2017).
- [52] L. Grünhaupt, M. Spiecker, D. Gusenkova, N. Maleeva, S. T. Skacel, I. Takmakov, F. Valenti, P. Winkel, H. Rotzinger, W. Wernsdorfer, A. V. Ustinov, and I. M. Pop, Granular aluminium as a superconducting material for high-impedance quantum circuits, *Nat. Mater.* **18**, 816 (2019).
- [53] P. Scarlino, D. J. van Woerkom, U. C. Mendes, J. V. Koski, A. J. Landig, C. K. Andersen, S. Gasparinetti, C. Reichl, W. Wegscheider, K. Ensslin, T. Ihn, A. Blais, and A. Wallraff, Coherent microwave-photon-mediated coupling between a semiconductor and a superconducting qubit, *Nat. Comm.* **10**, 3011 (2019).
- [54] S. Richer and D. DiVincenzo, Circuit design implementing longitudinal coupling: A scalable scheme for superconducting qubits, *Phys. Rev. B* **93**, 134501 (2016).
- [55] P. Rabl, P. Cappellaro, M. V. Gurudev Dutt, L. Jiang, J. R. Maze, and M. D. Lukin, Strong magnetic coupling between an electronic spin qubit and a mechanical resonator, *Phys. Rev. B* **79**, 041302(R) (2009).
- [56] P. Peng, C. Matthiesen, and H. Häffner, Hartmut, Spin readout of trapped electron qubits, *Phys. Rev. A* **95**, 012312 (2017).
- [57] M. Leib and M. J. Hartmann, Synchronized Switching in a Josephson Junction Crystal, *Phys. Rev. Lett.* **112**, 223603 (2014).
- [58] M. Leib, F. Deppe, A. Marx, R. Gross, and M. J. Hartmann, Networks of nonlinear superconducting transmission line resonators, *New J. Phys.* **14** 075024 (2012).
- [59] N. Samkharadze, A. Bruno, P. Scarlino, G. Zheng, D. P. DiVincenzo, L. DiCarlo, and L. M. K. Vandersypen, High-Kinetic-Inductance Superconducting Nanowire Resonators for Circuit QED in a Magnetic Field, *Phys. Rev. Applied* **5**, 044004 (2016).
- [60] L. S. Pontryagin, *The Mathematical Theory of Optimal Process* (New York: Interscience Publishers), 1962.